Materialia 4 (2018) 423–430

Contents lists available at ScienceDirect

Materialia

journal homepage: www.elsevier.com/locate/mtla

Full Length Article

Pore structure stabilization during the preparation of single phase ordered macroporous α-alumina

Jeroen E. van den Reijen[1], Petra H. Keijzer[1], Petra E. de Jongh*

Debye Institute for Nanomaterials Science, Utrecht University, Universiteitsweg 99, 3584CG Utrecht, The Netherlands

ARTICLE INFO

Keywords:
Alumina (α-Al_2O_3)
Porous material
Template synthesis
Long-range ordering
3DOM

ABSTRACT

Ordered porous materials are highly relevant for applications in fields such as catalysis, adsorption and chromatography. Strategies such as soft and hard templating are now routinely applied to prepare for instance ordered mesoporous silica. In other cases, most notably when several polymorphic phase transformations are involved, achieving high quality ordered oxides is challenging. We present a strategy for the preparation of ordered macroporous α-alumina with a high degree of pore order. The preparation is based on impregnation of ordered polymeric spheres with an alumina precursor. Most notably it involves a first heating step in inert atmosphere, leading to conversion of the polymeric template into carbon effectively delaying the phase transitions and stabilizing the pore structure up to high temperatures. A subsequent heat treatment in oxidative atmosphere then removes the carbon and ordered marcoporous α-alumina is obtained with circa 220 nm cages interconnected by windows of circa 105 nm, and a specific surface area of circa 25 $m^2\ g^{-1}$. Our method led to a strong preservation of the long-range order of the pore structure, as not only evidenced by electron microscopy, but also quantified by spectroscopy. High surface area α-alumina is of particular interest as a catalyst support, but the preparation method might also be extended to other ordered macroporous oxides that are difficult to prepare due to phase transitions such as TiO_2.

1. Introduction

Several important porous materials, such as zeolites and clays, occur naturally. However, a great step forward was the synthesis of new classes of porous materials in the laboratory. This started in the 1940 s with synthetic zeolites, which are now used on a wide scale as catalysts, softeners and adsorbents [1]. Zeolites are prepared by using small ions or molecules as templates during hydrothermal growth, and hence the pore sizes are typically in the microporous (< 2 nm) regime [1]. Another breakthrough was the first synthesis of ordered mesoporous (2–50 nm) silica (MCM-41), as reported in 1992 [2]. In this case, the mesoporous silica was formed around a template of micelles, consisting of long hydrocarbon chain surfactants or block copolymers [2–4]. The mesoporous materials do not consist of crystalline silica, but do have a very well defined pore ordering, and a very narrow pore size distribution. Some examples of applications of ordered mesoporous materials are chromatography, drug delivery and catalysis [5–8]. These ordered mesoporous systems also served as model systems to advance fundamental understanding, allowing advanced characterization and to systematically investigate the influence of parameters on catalyst synthesis and performance [9–12].

Using these soft templating methods, the pore size is limited by the size of the organic templates or their micelles, which goes up to roughly 10 nm, with a further extension to circa 30 nm by micelle swelling [4,13,14]. Porous materials with larger pore sizes, such as pores in the macroporous regime (> 50 nm), can be synthesized by using techniques such as foaming, emulsion templating or flame spray pyrolysis, [11,15–17] but in these cases the pore size distribution is usually wide and pore ordering is absent or poorly controlled. When ordered macroporous materials are desired, hard templates need to be used [18,19]. Velev et al. were the first to report on the preparation of three dimensionally ordered macroporous (3DOM) silica [20]. Polymer spheres self-assembled into a so called “colloidal crystal” were used as a sacrificial template, whereupon silica was grown in the voids of these colloidal crystals, followed by template removal. This method proved to work also for other three dimensional ordered macroporous materials, such as ZnO, Fe_2O_3 and Cr_2O_3 [21–25].

While 3DOM silica is relatively easily synthesized, the synthesis of ordered porous metal oxide phases that need a high temperature to be formed is challenging [26]. A notoriously difficult compound to synthesize is porous α-alumina, as illustrated for instance by Sadakane et al. who prepared a range of ordered materials, but failed to form ordered

* Corresponding author.
E-mail address: P.E.deJongh@uu.nl (P.E. de Jongh).
[1] Both the authors contributed equally to this work.

https://doi.org/10.1016/j.mtla.2018.10.016
Received 10 September 2018; Accepted 30 October 2018
Available online 2 November 2018

porous α-alumina [27]. α-alumina is the most stable alumina phase at high temperatures and can be formed from other alumina polymorphs above 1100 °C. The thermal stability and relatively low cost make α-alumina an attractive material for refractories, ceramics and abrasives [28–33]. In principle, due to its chemical and thermal inertness, α-alumina is also very attractive as a catalyst support, and indeed the support of choice for catalysts used in large industrial processes such as ethylene epoxidation over a supported silver catalyst [34–36]. However, in catalysis, large specific support surface areas (preferably > 10 $m^2\ g^{-1}$) are often crucial, while this is extremely difficult to achieve with α-alumina. Commercial α-alumina exhibits typically a specific surface area of only about 1 $m^2\ g^{-1}$, with 8 $m^2\ g^{-1}$ being the highest specific surface area reported [37–39]. The material goes through several crystal phase transitions to form α-alumina from alumina precursors or other alumina polymorphs, which leads to a severe loss in specific surface area [40–42].

Alternative preparation methods for the preparation of high surface α-alumina have been explored. In patent literature, a method is reported involving incorporation of a carbon template in γ-alumina followed by two thermal treatments, first in inert atmosphere to obtain α-alumina and a second treatment in oxidizing atmosphere to remove the carbon [39]. Similar methods were used by Martin-Ruiz et al., Pérez et al. and Furlan et al., in which alumina was formed in the presence of a polymer [43–45]. Using these methods, α-alumina with a specific surface area up to 70 $m^2\ g^{-1}$ was produced [39], but without a well-defined pore size or structure. As far as we are aware, the only successful synthesis of ordered macroporous α-alumina has been reported by Sokolov et al., who used self-assembled poly(methyl methacrylate) (PMMA) spheres as a sacrificial template [46]. Such a polymeric template cannot withstand high temperatures in air, but nevertheless ordered macroporous α-alumina was formed at higher temperatures (1150 °C), as apparently enough of the template remained during the heating to offer some stabilization of the structure during the phase transitions.

Inspired by these results, we designed a new strategy to prepare high surface area ordered macroporous α-alumina with a very high quality pore structure. We used self-assembled PMMA sphere crystals to start with as templates, converted the crystals in-situ into a protective carbon coating, followed by the formation of alumina in the presence of this protective carbon at higher temperatures but still in inert atmosphere. Subsequently, in a separate oxidative treatment step, the carbon coating was removed and full conversion to α-alumina took place. This strategy allows the formation of high quality ordered macroporous α-alumina material with specific surface areas of 25 $m^2\ g^{-1}$, as we evidence in this paper using detailed electron microscopy and reflectance spectroscopy.

2. Experimental section

2.1. Synthesis polymeric template

Poly(methyl methacrylate) (PMMA) spheres were synthesized by using the surfactant free emulsion polymerization of methyl methacrylate (MMA, 99%, ≤ 30 ppm 4-methoxyphenol inhibitor, Sigma-Aldrich) in water. Following the procedure of Zhou et al. and Schroden et al., 100 mL MMA and 400 mL demineralized water in a 1 L round bottom flask were stirred by an overhead stirrer at 450 rpm [47,48]. The emulsion was heated to 70 °C and nitrogen was bubbled through the emulsion for at least 30 min to remove dissolved oxygen from the dispersion and to deactivate the inhibitor. Thereafter, 69 mg potassium persulfate (KPS, initiator) was added, resulting in a 0.5 mM concentration. The emulsion was left to react for 3 h at 70 °C after which a white dispersion had formed.

The dispersion was allowed to cool down to room temperature and was filtered to remove larger chunks of polymer. The filtrate was centrifuged for 20 h at 3000 rpm during which a white solid precipitated. The clear supernatant was decanted, and the obtained white powder was left to dry for several days at room temperature in air after which it was crushed into a powder.

Table 1
Overview of the synthesis parameters for 3DOM alumina samples.

Sample	Heat treatment(s)	Number of impregnation steps
3DOM_1_air	Air	1
3DOM_4 _air	Air	4
3DOM_3_N2_air	Nitrogen and air	3

2.2. Ordered macroporous alumina

Three dimensionally ordered macroporous (3DOM) α-alumina was obtained by impregnation of the polymeric template with an alumina precursor [47,49]. In a typical synthesis, 1.5 g template powder was placed in a Buchner funnel and drop-wise approximately 3 mL solution of 1 M aluminum nitrate nonahydrate in demineralized water/methanol (1:1 vol ratio) was added to completely wet the template. After 2 min of soaking, a dynamic vacuum was applied for 20 min to remove excess solvent. Subsequently, the dry powder was wetted with 3 mL ammonia (28–30%)/methanol (1:1 vol ratio) to form aluminum hydroxide in the pores of the template. Again, the material was dried via vacuum suction for 20 min. In order to obtain sufficient filling of the pores, these steps were performed one, three or four times before drying the powder overnight at room temperature in air [47,49]. Note that to maximize the pore filling, each impregnation consisted out of two different steps; firstly, an impregnation with an $Al(NO_3)_3{\cdot}9H_2O$ solution and secondly a washing with an ammonia solution to form $Al(OH)_3$.

The once and four times impregnated template materials were calcined in a flow of air of at least 0.5 L min^{-1} (GHWV = 20 L $g_{template}{}^{-1}$ hr^{-1}), heated with a 5 °C min^{-1} heating ramp to 1150 °C and kept at this temperature for 6 h, in similar fashion to established procedures [46,47,49]. The resulting samples were labeled 3DOM_1_air and 3DOM_4_air, indicating the amount of impregnation steps and the gas atmosphere respectively (Table 1). 1.5 g of dry, three times impregnated material was heated under a nitrogen flow with a 5 °C min^{-1} heating ramp to 1150 °C and kept at this temperature for 6 hours. The resulting material was black, or dark blue/green and a second heat treatment in a flow of air with the same flow and temperature program was applied after which a pristine white powder was obtained. The resulting sample was labeled 3DOM_3_N2_air. For temperature studies, the impregnated material was heated separately in air or in nitrogen flow to 200 °C, 400 °C, 600 °C, 800 °C, 1000 °C and 1150 °C. As reference material, bulk aluminum hydroxide was prepared by mixing an equal amount of the above described aluminum nitrate and ammonia-methanol solutions without template present. This material was heated in air flow to 200 °C, 400 °C, 600 °C, 800 °C, 1000 °C and 1150 °C.

2.3. Characterization

The polymer template and 3DOM powders were analyzed using Scanning Electron Microscopy (SEM) with a FEI XL30 FEG operated at 15 kV, and FEI Helios G3 UC operated at 2 kV. The micrographs were processed using iTEM Soft Imaging System software [50]. Diffuse-Reflectance UV/Vis spectra of the PMMA powder and the 3DOM materials were obtained using a Varian CARY 500 Scan UV/Vis-NIR spectrophotometer with an integrating sphere detector. In a typical analysis of the 3DOM materials, 30 mg of analyte was diluted with 600 mg pristine α-Al_2O_3 (1 $m^2\ g^{-1}$, 100 mesh, Sigma-Aldrich) and ground into a fine powder before taking a spectrum of the 1000–200 nm range. A background measurement of pristine α-Al_2O_3 was taken which was automatically subtracted from the obtained spectrum.

Crystal phase analysis was performed with X-Ray Diffraction (XRD) on a Bruker D8 Phaser diffractometer equipped with a Co Kα source

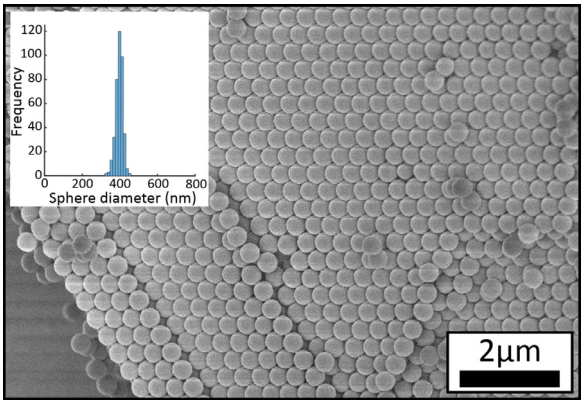

Fig. 1. SEM image of PMMA spheres ordered in a colloidal crystal after centrifugation with histogram of the particle size distribution in the inset. Average particle size was 400 ± 24 nm respectively.

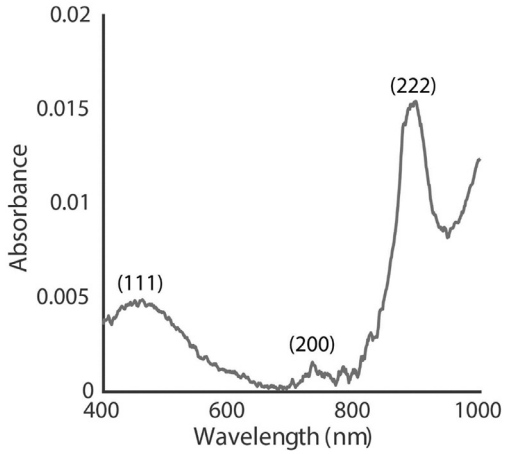

Fig. 2. DR UV/Vis spectrum of the template with peaks corresponding to 400 nm PMMA spheres in a colloidal crystal. Peak positions at 450, 780 and 900 nm correspond to (111), (200) and (222) plane reflections of the PMMA spheres, respectively.

($\lambda = 0.1789$ nm) using an angle range from 20° to 90° in 2θ and comparing XRD diffractograms with the PDF-4 + 2016 database. Crystallite sizes were estimated using the Scherrer equation [51,52].

Nitrogen physisorption isotherms were measured at −196 °C on a Micromeritics TriStar 3000 apparatus. The specific surface area of the support was calculated using the BET equation ($0.05 < p/p^0 < 0.25$). Mercury porosimetry was performed using a Micromeritics AutoPore IV 9500 in the Chemical Reactor Engineering group at the Eindhoven University of Technology. Pore volume data were calculated over the range 0.0007–227.5270 MPa, assuming a contact angle between the support materials and the mercury of 130° and mercury surface tension and density of 485 dynes cm^{-1} and 13.5335 g cm^{-3}, respectively.

3. Results and discussion

3.1. Polymer template

In Fig. 1, a Scanning Electron Microscopy (SEM) image of the polymeric template after centrifugation and drying is shown. In the inset, a histogram of the sphere diameter is added. The average sphere size is 400 ± 24 nm. The monodispersity of the particle sizes can be seen from the histogram and from visual inspection of the image. The deposition of the spheres was relatively slow, allowing the formation of a hexagonally ordered structure (a "crystal") as a close packing minimizes the energy of the system.

Diffuse-reflectance (DR) UV/Vis spectroscopy showed that the closed packed ordering of the polymer spheres is not only present at the surface, but also at the center of the colloidal crystal particles. In the DR UV/Vis spectrum (Fig. 2), three peaks are visible. Assuming a closed packed ordering of the polymer spheres, the two most intense peaks at 895 and 450 nm are assigned to second and first order diffraction of the nearest neighbor spheres in a close packed structure ((222) and (111) crystal planes), while the least intense peak (780 nm) corresponds to the second order next nearest neighbor diffraction (200). By assuming a closed packed crystal structure, an average sphere diameter of 404 ± 20 nm was calculated, which is in agreement with the particle size measured with SEM and dynamic light scattering (Supplementary Information, Section S1).

3.2. The formation of macroporous α-alumina

The polymeric template was used to synthesize macroporous α-alumina. However, upon decomposition of aluminum hydroxide at 400 °C, first γ-alumina is expected to form, while α-alumina should be formed above 1100 °C [40,53]. When bulk alumina hydroxide without any template is heat treated in a similar procedure, we indeed observe the formation of both phases at the expected temperatures (Supplementary Information, Section S2).

Upon heat treatment of the impregnated template in air, the aluminum hydroxide in the voids of the template decomposes and the template is burned off. To understand the effect of the confinement of the hydroxide on the phase transitions, we first evaluated the crystalline phases of alumina in the voids of the template using X-Ray Diffraction (XRD). In the left frame of Fig. 3, the diffractograms of the composite treated in air at different temperatures are shown. At the bottom of the frame, the diffractogram of the impregnated template before heating is shown, displaying two broad diffraction peaks attributed to the PMMA polymer [54]. With increasing temperature, both the aluminum hydroxide and the polymer peaks disappear and at 600 °C, no diffraction peaks are visible. Broad peaks from γ-alumina appear at 800 °C [43,55]. The broad diffraction peaks indicate that the material consists of relatively small crystallites with sizes of 5 ± 1 nm. These peaks disappear in favor of peaks that are attributed to crystalline α-alumina, which sharpen upon heating to 1150 °C.

The disappearance of the broad diffraction peaks attributed to the polymeric material at 200–400 °C is in accordance with TGA-MS of the material (Supplementary Information, Section S2, Fig. S3), showing that in this temperature range, the template is burned off. The presence of γ-alumina at 800 °C and α-alumina above 1000 °C is in accordance with the XRD analysis of bulk aluminum hydroxide (Supplementary Information, Section S2, Fig. S4) and the alumina phase diagram [56,57]. However, compared to the bulk material, the conversion of confined aluminum hydroxide in the voids of the template into γ-alumina is delayed by 400 °C. We believe that this delay is caused by residual template material present at least up to 600 °C.

In the right frame of Fig. 3, the diffractograms of the impregnated template heat treated under nitrogen flow are shown. The diffractogram of the composite heated to 200 °C is very similar to the diffractogram taken before heat treatment. By heating the composite in nitrogen flow, the decomposition of the polymeric template is delayed compared to when the composite is heat treated in air. When the composite is treated to 400 °C, these broad peaks have disappeared and after heating to 600 °C, another broad peak is visible at 30° 2Θ. This peak was not observed in the material treated in air and is attributed to a carbon material, formed due to pyrolysis of the polymer template. The broad peak is still present in the composite heated at 800 °C, and next to this peak, no other peaks are visible.

The appearance of γ-alumina is delayed to 1000 °C and this phase is still present after heat treatment at 1150 °C. Even after prolonged

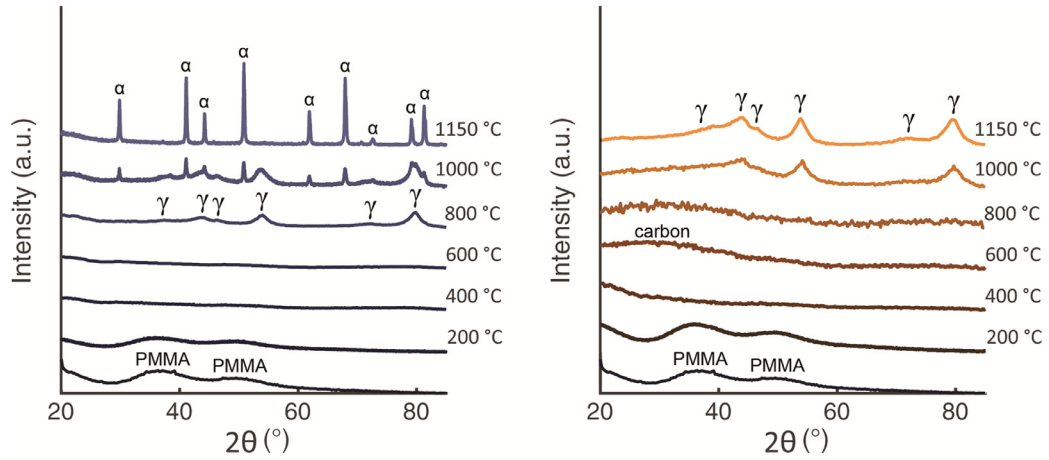

Fig. 3. Stacked diffractograms of the impregnated template treated at different temperatures in air (left) and under nitrogen flow (right). After the material was treated at 800 °C in air, γ-alumina was formed, converting into α-alumina at higher temperatures. Under inert atmosphere, the formation of γ-alumina was delayed to even much higher temperatures and no α-alumina was yet formed at 1150 °C.

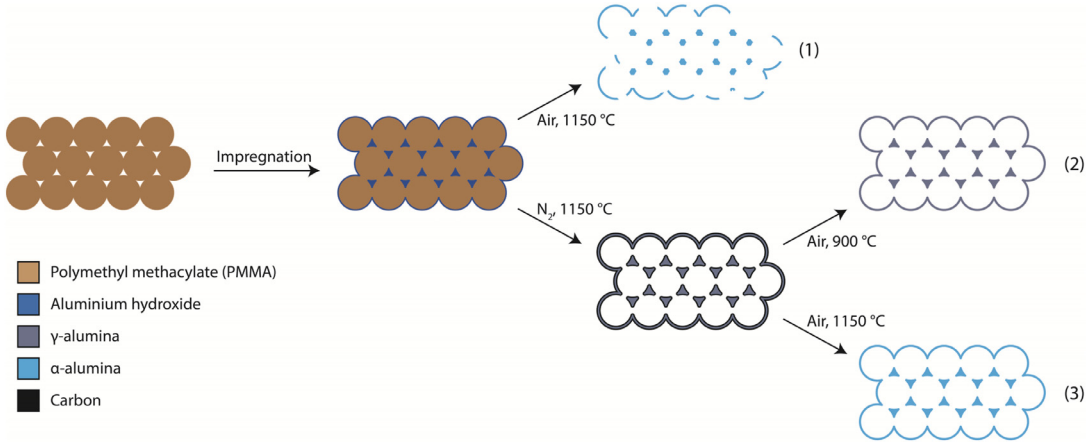

Fig. 4. Schematic representation of the synthesis procedures of 3DOM α-alumina by reference procedure (1) and the procedures described in this paper for 3DOM γ-alumina (2) and 3DOM α-alumina (3).

heating (6 h) at 1150 °C, no crystalline α-alumina was observed. We postulate that the delay in phase transitions is caused by the presence of the formed carbon. Causing a delay in a phase transition is only possible when the carbon and alumina are in close contact. This ensures that carbon can act as a protective layer to stabilize the pore structure even at 1150 °C. The pyrolysis of the template material into a protective carbon coating is supported by the black color after the heat treatment in nitrogen flow at 1150 °C (Supplementary Information, Section S2, Fig. S2). Since at this temperature no α-alumina was formed, carbon free 3DOM γ-alumina with a high-quality pore structure can be obtained by simply burning off the carbon at 900 °C in an oxidizing atmosphere (route 2 in Fig. 4 and Supplementary Information, Section S3). Alternatively, the carbon-coated γ-alumina can be used as a ceramic with altered dielectric properties [58]. Next to the ordered macropores, also some pores in the range of 30–90 μm were present in the obtained γ-alumina. The surface area of this material was 85 ± 10 $m^2\ g^{-1}$. By increasing the temperature of the second heat treatment in oxidizing atmosphere to 1150 °C, 3DOM α-alumina was formed (route 3 in Fig. 4 and Supplementary Information, Section S2, Fig. S5). Although the carbon was burned off before the transformation of γ-alumina to α-alumina, the pore structure was well preserved in the α-alumina, better than in the case of treating impregnated template material in oxidizing atmosphere directly (route 1 in Fig. 4), as will be discussed in more detail below.

By increasing the amount of impregnation steps, the yield of the ordered macroporous material was increased. The synthesis of the reference material (3DOM_1_air) yielded 20 ± 1 mg $g_{template}^{-1}$, which corresponds to circa 2% of the total pore volume of the template material being filled. The yields for 3DOM_4_air and 3DOM_3_N_2_air were 40 and 30 mg $g_{template}^{-1}$, respectively, and are hence significantly higher. Increasing the number of impregnation steps clearly increases the yield of this procedure, but cannot lead to full pore filling with alumina, as the volume of the precursor ($Al(NO_3)_3{\cdot}9H_2O$) is much higher than the volume of its decomposition product, $Al(OH)_3$, and the final alumina phase. When taking this decrease in volume into account, the maximum achievable yield (assuming 100% pore filling using a single impregnation with $Al(NO_3)_3{\cdot}9H_2O$) is 63 mg $g_{template}^{-1}$. After 4 impregnation steps, we reached 60% of this theoretical value.

3.3. Quality of the pore structure

A crucial part of our strategy for improving the quality of the ordering and pore structure is by stabilizing the morphology by pyrolysis of the template material into a protective carbon coating. Next to that, we investigated the effect of increasing the amount of impregnation steps on the quality of the pore structure. Several techniques were applied to investigate the effect of our strategy on the quality of the prepared macroporous α-alumina. Nitrogen physisorption and mercury intrusion measurements on 3DOM_3_N_2_air (Supplementary Information, Section S4) showed a specific surface area of 25 ± 10 $m^2\ g^{-1}$, originating from macropores, while micro- and mesopores are absent. This is a very high

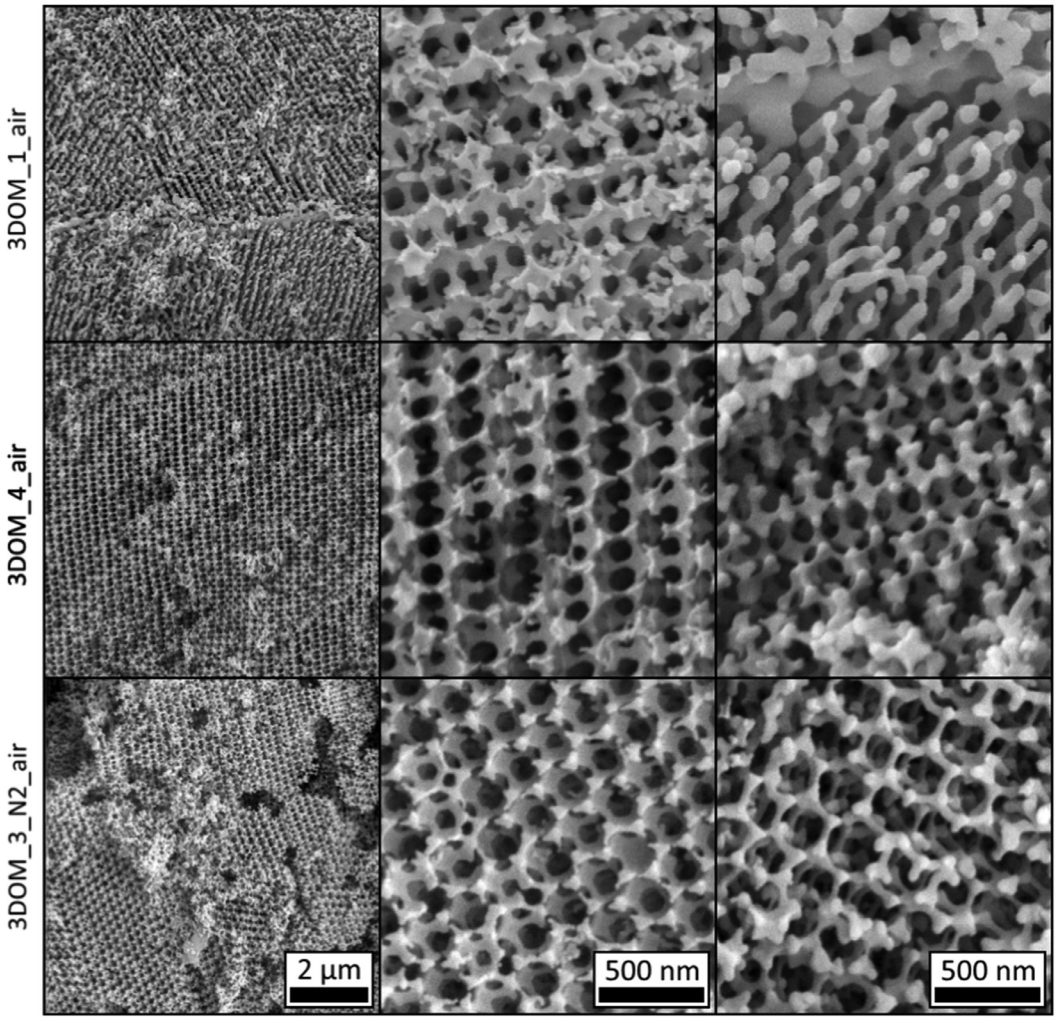

Fig. 5. SEM images of macroporous α-alumina 3DOM_1_air (top), 3DOM_4_air (middle) and 3DOM_3_N2_air (bottom). In 3DOM_3_N2_air, pores of 220 ± 15 nm are connected by windows of circa 105 ± 5 nm, resulting in a cage structured material. For 3DOM_4_air and 3DOM_1_air, cage structure is not as good preserved, as alumina migrated from the walls of the cages to form pillars.

specific surface area for α-alumina materials and in good agreement with the theoretical expected value of 14 m^2 g^{-1} for the hexagonal ordered macroporous structure (Supplementary Information, Section S4).

In Fig. 5, SEM images of 3DOM_1_air, 3DOM_4_air and 3DOM_3_N_2_air are shown. The frames in the left column give an overview of the material, while the middle and the right frames show images taken at higher magnifications. We tried to show both the best (middle column) and the worst parts (right column) of the samples. In the left frame on the top row, long-range ordering in the 3DOM_1_air sample is visible in the overview image. However, the material in this frame consists of sheets of alumina instead of the expected cage-structure, as can be better observed at higher magnifications (right frame). In the middle frame, a higher magnification of another section of the material does show the expected morphology, but this morphology co-exists with the sheets visible in the overview and at higher magnification in the right frame. These observations suggest that the sheets originate from the cage structure, which deformed during phase transitions at high temperature as also observed in the original paper by Sokolov et al. [46].

In the middle row of frames, 3DOM_4_air is displayed. The left frame shows the desired hexagonal cage-structure, although in the middle frame of this row, the cage structure appears to be slightly split, forming an intermediate morphology between the sheets observed in the 3DOM_1_air sample and the desired cage morphology. In the right frame, no sheets are visible, but also no fully formed cages are observed. The material resembles a stick-and-node structure, with some absent sticks on the surface of the material, similar to observations from Rudisill et al. [26]. In the bottom row, showing the sample prepared by the two-step approach, the cage structure of 3DOM_3_N_2_air is visible throughout the sample (left frame) and a clear hexagonal ordering is visible at higher magnifications (middle frame). Even for those parts of the material in which the morphology is least preserved, the cages of the material are enclosed by a well-defined stick-and-node structure, and the cage structure is overall preserved.

From SEM it appears that increasing the amount of impregnation steps increases the quality pore structure of the final macroporous α-alumina in comparison to the 3DOM_1_air sample. In the images in Fig. 5, the loss of the desired cage structure in these samples seems to result from the transport of the alumina from the thin to the thicker sections of the cage morphology, resulting in a loss of the cage morphology [26,46,59–61]. This transport towards the thicker parts of the structure is driven by the minimization of the surface area. A comparable loss of pore structure was observed for other microporous matrials [26,59]. In the worst case, this transport results in some cages no longer having a wall separating them, or in the formation of α-alumina sheets.

When following our new strategy, the ordered macroporous structure is supported by the protective carbon coating, such as in 3DOM_3_N_2_air, and the resulting material retains the cage structure

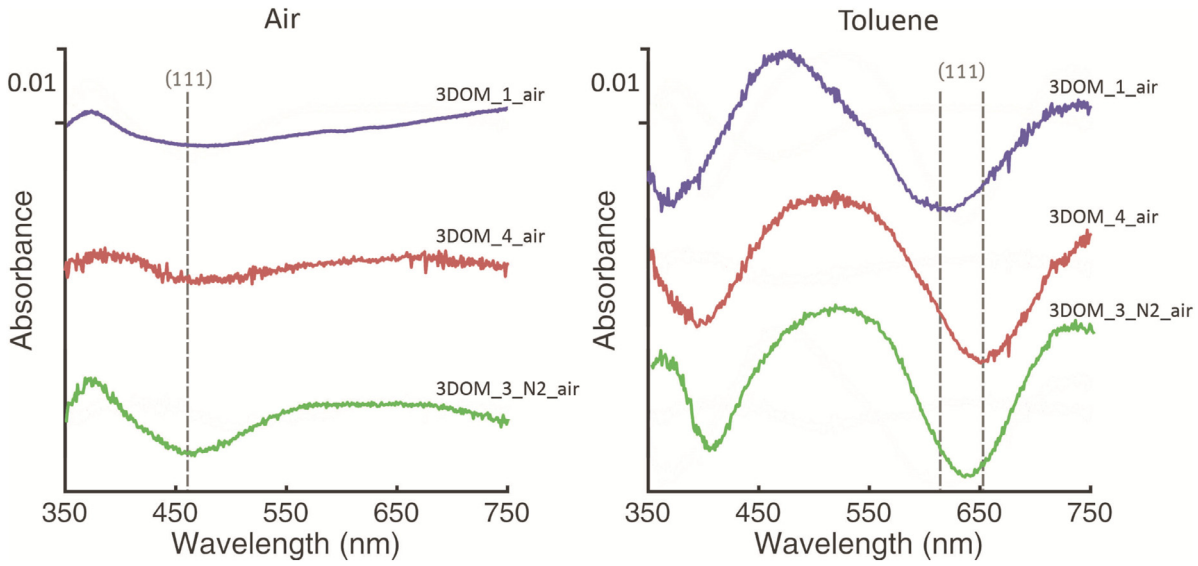

Fig. 6. Stacked DR UV/Vis spectra of macroporous α-alumina 3DOM_1_air (top, purple), 3DOM_4_air (middle, red) and 3DOM_3_N2_air (bottom, green) in air (left) and toluene (right). A redshift of the reflection minima is observed in toluene due to a change in refractive index.

and the pore structure is far better than if this carbon coating had not been formed. While the morphology is maintained to a higher degree, the different preparation routes do not have a significant influence on the pores sizes. An average pore size of circa 220 ± 15 nm was measured. The windows and walls are respectively 105 ± 5 nm and 35 ± 5 nm. The pore sizes are significantly smaller in the resulting macroporous material than the size of the polymer template (400 nm spheres). For all three samples, the reduction of the pore size is similar as they are derived from the same template material. Additional SEM, focused ion beam (FIB)-SEM and transmission electron microscopy (TEM) images in which the pore structure at larger scale and the pore structure on the inside of the particle are visualized are given in the Supplementary Information, Section S4, Fig. S10 and S11.

While electron microscopy can illustrate the degree of ordering and how well the desired morphology is maintained, a reliable and statistically relevant method is required to validate these results. Ordering in the macroporous material results in peaks in DR UV/Vis spectra [17,47,58,62,63]. The position of these reflectance peaks reflects the size of the unit cell, the morphology of the ordered structure and the average refractive index of the sample. The latter is determined by the relative amounts of the material (volume fraction), in this case α-alumina, and the liquid or gas in the pores of the structure. The dependencies can be expressed in the Bragg equation (Eq. (1) and Supplementary Information, Section S1, Eq. S5). In this equation, the interplanar distance is represented by d_{hkl}, the peak position as λ, the diffraction order as m and the average refractive index as $n_{material,\ avg}$. The width and intensity of peak is determined by the quality of the ordered structure.

$$D = \frac{m\lambda}{2d_{hkl}n_{material,avg}} \quad (1)$$

In Fig. 6, the DR UV/Vis spectra of the three 3DOM α-alumina's (3DOM_1_air, 3DOM_4_air and 3DOM_3_N2_air) are shown. Results from the samples measured in air are shown in the left frame. The positions of the reflectance peaks in this frame in are similar for all three samples. The reflectance peaks of 3DOM_1_air and 3DOM_4_air spectra do not differ visibly, both exhibiting a shallow peak at 500 nm. The spectrum of 3DOM_3_N_2_air exhibits a sharp peak at the same position.

To allow for a better distinction between the spectra of the three samples, especially between the 3DOM_1_air and 3DOM_4_air samples, the DR UV/Vis spectra of these samples were also measured after filling the pores with toluene (right frame of Fig. 6). When the spectrum is measured in toluene, the reflectance peaks are more intense and redshifted, due to the higher density of toluene compared to air and the larger refractive index (Supplementary Information, Section S1, Eq. S5), respectively. The (111) reflection peaks that were visible when the measurements were performed in air (left frame) are shifted to 600–650 nm while additional peaks for (220) reflections appear at 350–400 nm, due to this redshift. The redshift in 3DOM_1_air is less than the shift in the two other materials and similarly, the reflectance peaks of 3DOM_1_air are clearly less sharp and less intense than the peaks from both 3DOM_4_air (red) and 3DOM_3_N_2_air (green).

As shown by Blanford et al., from the red shift of the refractive peak, a number of material characteristics can be derived, which together with the full width at half maximum (FWHM) describe the quality of the morphology of the material [63]. These characteristics are summarized for the three 3DOM α-alumina's in Table 2. Using the position of the d_{111} reflectance peak in air ($n = 1$), butanol ($n = 1.3991$, Supplementary Information, Section S4, Fig. S14) and toluene ($n = 1.4941$), the interplanar distance (d_{111}) and the volume fraction of alumina (φ) can be calculated using the linearized Bragg equation (Eq. (2)), while the cage size (D) can in turn be derived from the interplanar distance (Supplementary Information, Section S1) [63]. In this equation, the d_{hkl} peak position (λ), diffraction order (m), volume fraction solid material (φ) and refractive index of the solid wall (n) are represented. The refractive index of the wall is assumed to be 1.7682, equal to the refractive index of bulk α-alumina [64].

$$\lambda = \frac{2d_{hkl}}{m}\varphi n_{wall} + \frac{2d_{hkl}}{m}(1-\varphi)n_{solvent} \quad (2)$$

No significant increase in the volume fraction and the cage sizes was observed with increasing impregnation steps (Table 2). Taking into account that with SEM the pore size was measured, but with using DR UV/Vis the calculated size includes the wall thickness (of 35 ± 5 nm), the sizes measured with the different techniques are in good agreement.

Most importantly, the full width at half maximum (FWHM) of the refractive peak is a measure for the degree of ordering of the porosity in the material. A sharp peak is indicative of a better ordered material. The decrease in FWHM with both the amount of impregnation steps and the additional protective carbon coating is striking. This decrease shows that both adjustments result in better ordering compared to the 3DOM_1_air reference material. The FWHM for 3DOM_3_N_2_air is even similar to the FWHM of ordered macroporous γ-alumina in methanol described in literature [63]. Hence this suggests that with our new two-step approach α-alumina can be made with a similarly high quality as

Table 2
Material characteristics for 3DOM support materials, derived from DR UV/Vis in different solvents (air, butanol and toluene) and Eq. (2).

Sample	3DOM_1_air	3DOM_4 _air	3DOM_3_N2_air[a]
Volume fraction of alumina, φ	0.18 ± 0.02	0.14 ± 0.01	0.16 ± 0.02
Interplanar spacing, d_{111} [nm]	206	208	211
Calculated cage (+ wall) size, D [nm][b]	252	255	259
FWHM in toluene [cm^{-1}]	3433	2700	2286

[a] 3DOM_3_N2_air measured in air, butanol, methanol and toluene.
[b] Assuming closed packed arrangement of the pores.

the γ-alumina of Blanford et al., despite the extra phase transformation step.

Having a very high surface area α-alumina support is of particular interest in catalysis, as it is notoriously difficult to obtain such high surface areas by known methods. High surface areas serve to better stabilize the active supported metal particles, even more so if the pore structure is cagelike [55,65]. The preparation strategy proposed in this paper could be relevant also for other ordered macroporous materials that are difficult to prepare due to phase transitions, such as TiO_2 [66,67].

4. Conclusion

We demonstrate a method for the synthesis of high quality, high surface area ordered macroporous α-alumina, based on impregnation with aluminum hydroxide of an ordered polymer template. Multiple impregnating steps contribute to a high degree of pore filling with aluminum hydroxide, increasing the yield of the synthesis and minimizing the loss of ordering. We employed a specific heat treatment in inert atmosphere to convert the polymeric template into a protective carbon coating. Close contact of the protective carbon coating with the alumina surface caused a delay of the alumina phase transitions to higher temperatures and helped to preserve the pore structure. By a final heat treatment in air, the carbon was removed, and high quality ordered macroporous α-alumina with a specific surface area of circa 25 m^2 g^{-1} was obtained. The high quality of the pore structure was evidenced by electron microscopy and quantified by spectroscopic analysis.

Funding sources

This work was supported by an NWO Vici project 16.130.344 (JvR and PdJ) and by the Netherlands Center for Multiscale Catalytic Energy Conversion (MCEC), an NWO Gravitation programme funded by the Ministry of Education, Culture and Science of the government of the Netherlands (PK).

Associated content

The following files are available free of charge. Word file with supporting information: Calculations of particle size from diffuse reflectance UV/Vis, the effect of heat treatment in air and nitrogen and additional analysis results on γ- and α-alumina materials.

Declaration of interests

The authors declare that they have no known competing financial interests or personal relationships that could have appeared to influence the work reported in this paper.

Acknowledgment

The authors would like to thank Peter Lipman of Chemical Reactor Engineering, Eindhoven University of Technology for performing mercury intrusion experiments, Marjan Versluijs-Helder and Jochem Wijten of Utrecht University for performing SEM analysis and Mies van Steenbergen of Pharmaceutics, Utrecht University for performing TGA and DLS analysis.

Supplementary materials

Supplementary material associated with this article can be found, in the online version, at doi:10.1016/j.mtla.2018.10.016.

References

[1] C.S. Cundy, P.A. Cox, The hydrothermal synthesis of zeolites: history and development from the earliest days to the present time, Chem. Rev. 103 (2003) 663–701, doi:10.1021/cr020060i.
[2] C.T. Kresge, M.E. Leonowicz, W.J. Roth, J.C. Vartuli, J.S. Beck, Ordered mesoporous molecular sieves synthesized by a liquid-crystal template mechanism, Nature 359 (1992) 710–712, doi:10.1038/359710a0.
[3] D. Zhao, Q. Huo, J. Feng, B.F. Chmelka, G.D. Stucky, Nonionic triblock and star diblock copolymer and oligomeric surfactant syntheses of highly ordered, hydrothermally stable, mesoporous silica structures, J. Am. Chem. Soc. 120 (1998) 6024–6036, doi:10.1021/ja974025i.
[4] D. Zhao, Y. Wan, W. Zhou, Synthesis approach of mesoporous molecular sieves, Ordered Mesoporous Material, Wiley-VCH Verlag GmbH & Co. KGaA, 2013, pp. 5–54.
[5] F. Tang, L. Li, D. Chen, Mesoporous silica nanoparticles: synthesis, biocompatibility and drug delivery, Adv. Mater. 24 (2012) 1504–1534, doi:10.1002/adma.201104763.
[6] K.W. Gallis, J.T. Araujo, K.J. Duff, J.G. Moore, C.C. Landry, The use of mesoporous silica in liquid chromatography, Adv. Mater. 11 (1999) 1452–1455 doi:10.1002/(SICI)1521-4095(199912)11:17<1452::AID–ADMA1452>3.0.CO;2-R.
[7] M.E. Davis, Ordered porous materials for emerging applications, Nature 417 (2002) 813–821, doi:10.1038/nature00785.
[8] T. Maschmeyer, F. Rey, G. Sankar, J.M. Thomas, Heterogeneous catalysts obtained by grafting metallocene complexes onto mesoporous silica, Nature 378 (1995) 159–162, doi:10.1038/378159a0.
[9] G. Prieto, M. Shakeri, K.P. de Jong, P.E. de Jongh, Quantitative relationship between support porosity and the stability of pore-confined metal nanoparticles studied on CuZnO/SiO2 methanol synthesis catalysts, ACS Nano 8 (2014) 2522–2531, doi:10.1021/nn406119j.
[10] G. Prieto, J.D. Meeldijk, K.P. de Jong, P.E. de Jongh, Interplay between pore size and nanoparticle spatial distribution: consequences for the stability of CuZn/SiO2 methanol synthesis catalysts, J. Catal. 303 (2013) 31–40, doi:10.1016/j.jcat.2013.02.023.
[11] P.I. Ravikovitch, A.V. Neimark, Characterization of Nanoporous materials, Colloids Surf. A Physicochem. Eng. Asp. 187–188 (2001) 11–21. http://coewww.rutgers.edu/~aneimark/PDFs/COLSUA2001.PDF.
[12] K. Cychosz, X. Guo, W. Fan, R. Cimino, Characterization of the pore structure of three-dimensionally ordered mesoporous carbons using high resolution gas sorption, Langmuir 28 (2012) 12647–12654, doi:10.1021/la302362h.
[13] D. Zhao, Y. Wan, W. Zhou, Mechanisms for formation of mesoporous materials, Ordered Mesoporous Material, 2013, pp. 55–116.
[14] P. Yang, D. Zhao, D. Margolese, Block copolymer templating syntheses of mesoporous metal oxides with large ordering lengths and semicrystalline framework, Chem. Mater. (1999) 2813–2826. http://pubs.acs.org/doi/abs/10.1021/cm990185c. Accessed 28 March 2014.
[15] R.M. Laine, J.C. Marchal, H.P. Sun, X.Q. Pan, Nano-α-Al2O3 by liquid-feed flame spray pyrolysis, Nat. Mater. 5 (2006) 710–712, doi:10.1038/nmat1711.
[16] L.P. Lefebvre, J. Banhart, D.C. Dunand, Porous metals and metallic foams: current status and recent developments, Adv. Eng. Mater. 10 (2008) 775–787, doi:10.1002/adem.200800241.
[17] M. Abdullah, F. Iskandar, S. Shibamoto, T. Ogi, K. Okuyama, Preparation of oxide particles with ordered macropores by colloidal templating and spray pyrolysis, Acta Mater. 52 (2004) 5151–5156, doi:10.1016/j.actamat.2004.07.021.
[18] H. Nishihara, T. Kyotani, Templated nanocarbons for energy storage, Adv. Mater. 24 (2012) 4473–4498, doi:10.1002/adma.201201715.
[19] N.D. Petkovich, A. Stein, Controlling macro- and mesostructures with hierarchical porosity through combined hard and soft templating, Chem. Soc. Rev. 42 (2013) 3721–3739, doi:10.1039/C2CS35308C.

[20] O.D. Velev, T.A. Jede, R.F. Lobo, A.M. Lenhoff, Porous silica via colloidal crystallization, Nature 389 (1997) 447–448, doi:10.1038/38921.
[21] A. Stein, Sphere templating methods for periodic porous solids, Microporous Mesoporous Mater. 44–45 (2001) 227–239, doi:10.1016/S1387-1811(01)00189-5.
[22] A. Stein, R.C. Schroden, Colloidal crystal templating of three-dimensionally ordered macroporous solids: materials for photonics and beyond, Curr. Opin. Solid State Mater. Sci. 5 (2001) 553–564, doi:10.1016/S1359-0286(01)00022-5.
[23] X. Chen, Z. Li, J. Ye, Z. Zou, Forced impregnation approach to fabrication of large-area, three-dimensionally ordered macroporous metal oxides, Chem. Mater. 22 (2010) 3583–3585, doi:10.1021/cm100751w.
[24] G.R. Yi, J.H. Moon, S.M. Yang, Ordered macroporous particles by colloidal templating, Chem. Mater. 13 (2001) 2613–2618, doi:10.1021/cm0102584.
[25] H. Yan, C.F. Blanford, B.T. Holland, W.H. Smyrl, A. Stein, General synthesis of periodic macroporous solids by templated salt precipitation and chemical conversion, Chem. Mater. 12 (2000) 1134–1141, doi:10.1021/cm9907763.
[26] S.G. Rudisill, Z. Wang, A. Stein, Maintaining the Structure of templated porous materials for reactive and high-temperature applications, Langmuir 28 (2012) 7310–7324, doi:10.1021/la300517g.
[27] M. Sadakane, T. Horiuchi, N. Kato, C. Takahashi, W. Ueda, Facile preparation of three-dimensionally ordered macroporous alumina, iron oxide, chromium oxide, manganese oxide, and their mixed-metal oxides with high porosity, Chem. Mater. 19 (2007) 5779–5785, doi:10.1021/cm071823r.
[28] R.G. Munro, Evaluated material properties for a sintered alpha-alumina, J. Am. Ceram. Soc. 80 (1997) 1919–1928, doi:10.1111/j.1151-2916.1997.tb03074.x.
[29] C. Sadik, I.E. El Amrani, A. Albizane, Recent advances in silica-alumina refractory: a review, J. Asian Ceram. Soc. 2 (2014) 83–96, doi:10.1016/j.jascer.2014.03.001.
[30] J.J. Amero, Sintered Alpha-Alumina and Zirconia Abrasive Product and Process, US3454385, 1969.
[31] S.L. Conwell, W.P. Wood, Alpha Alumina-based Abrasive Grain, US5516348, 1996.
[32] M.J. Udy, Preparation of Refractory products, US271822, 1956.
[33] N. Setter, R. Waser, Electroceramic materials, Acta Mater. 48 (2000) 151–178 doi:10.1016/S1359-6454(99)00293-1.
[34] M.O. Özbek, R.A. van Santen, The mechanism of ethylene epoxidation catalysis, Catal. Lett. 143 (2013) 131–141, doi:10.1007/s10562-012-0957-3.
[35] M. Mitsuhata, F. Watanabe, T. Kumazawa, Silver Catalyst for Production of Ethylene Oxide, US4,368,144, 1983.
[36] R.P. Nielsen, J.H. La Rochelle, Catalyst for Production Of Ethylene Oxide, US3962136, 1976.
[37] C.-F. Mao, M. Albert Vannice, High surface area α-aluminas III. Oxidation of ethylene, ethylene oxide, and acetaldehyde over silver dispersed on high surface area α-alumina, Appl. Catal. A Gen. 122 (1995) 61–76 doi:10.1016/0926-860X(94)00214-2.
[38] J.N. Pattison, Low Surface Area Alpha Alumina Catalyst Support for the Selective Hydrogenation of Hydrocarbons, US3068303, 1962.
[39] L.L. Murrell, D.C. Grenoble, J.P. DeLuca, Process for Preparing Ultra-Stable, High Surface Area Alpha-Alumina, US4169883, 1976.
[40] R. van Santen, P. van Leeuwen, J. Moulijn, B.A. Averill, Preparation of catalyst support supports, zeolites and mesoporous materials, Catalan An Integral Approach, 1999, pp. 433–457.
[41] M. Nguefack, A.F. Popa, S. Rossignol, C. Kappenstein, Preparation of alumina through a sol–gel process. Synthesis, characterization, thermal evolution and model of intermediate boehmite, Phys. Chem. Chem. Phys. 5 (2003) 4279–4289, doi:10.1039/B306170A.
[42] J.G. Li, X. Sun, Synthesis and sintering behavior of a nanocrystalline α-alumina powder, Acta Mater. 48 (2000) 3103–3112, doi:10.1016/S1359-6454(00)00115-4.
[43] M.M. Martín-Ruiz, L.A. Pérez-Maqueda, T. Cordero, V. Balek, J. Subrt, N. Murafa, J. Pascual-Cosp, High surface area α-alumina preparation by using urban waste, Ceram. Int. 35 (2009) 2111–2117, doi:10.1016/j.ceramint.2008.11.011.
[44] K.P. Furlan, R.M. Pasquarelli, T. Krekeler, M. Ritter, R. Zierold, K. Nielsch, G.A. Schneider, R. Janssen, Highly porous α-Al2O3 ceramics obtained by sintering atomic layer deposited inverse opals, Ceram. Int. 43 (2017) 11260–11264, doi:10.1016/j.ceramint.2017.05.176.
[45] L.L. Pérez, V. Zarubina, H.J. Heeres, I. Melián-Cabrera, Condensation-enhanced self-assembly as a route to high surface area α-aluminas, Chem. Mater. 25 (2013) 3971–3978, doi:10.1021/cm401443b.
[46] S. Sokolov, D. Bell, A. Stein, Preparation and Characterization of macroporous α-Alumina, J. Am. Ceram. Soc. 86 (2003) 1481–1486, doi:10.1111/j.1151-2916.2003.tb03500.x.
[47] R.C. Schroden, M. Al-daous, C.F. Blanford, A. Stein, Optical properties of inverse opal photonic crystals, Chem. Mater. 14 (2002) 3305–3315.
[48] D. Zou, S. Ma, R. Guan, M. Park, L. Sun, J.J. Aklonis, R. Salovey, Model filled polymers V. Synthesis of crosslinked monodisperse polymethacrylate beads, J. Polym. Sci. Part A Polym. Chem. 30 (1992) 137–144, doi:10.1002/pola.1992.080300118.
[49] B. Holland, C. Blanford, A. Stein, Synthesis of macroporous minerals with highly ordered three-dimensional arrays of spheroidal voids, Science 281 (1998) 538–540. (80-.) http://www.sciencemag.org/content/281/5376/538.short . Accessed 28 March 2014.
[50] J. Hoekstra, A.M. Beale, F. Soulimani, M. Versluijs-Helder, J.W. Geus, L.W. Jenneskens, Shell decoration of hydrothermally obtained colloidal carbon spheres with base metal nanoparticles, N. J. Chem. 39 (2015) 6593–6601, doi:10.1039/C5NJ00804B.
[51] P. Scherrer, Bestimmung der inneren Struktur und der Größe von Kolloidteilchen mittels Röntgenstrahlen, Kolloidchem. Ein Lehrb., Springer Berlin Heidelberg, Berlin, Heidelberg, 1912, pp. 387–409, doi:10.1007/978-3-662-33915-2_7.
[52] J.I. Langford, A.J.C. Wilson, Scherrer after sixty years: a survey and some new results in the determination of crystallite size, J. Appl. Crystallogr. 11 (1978) 102–113, doi:10.1107/S0021889878012844.
[53] K. Wefers, C. Misra, Oxides and Hydroxides Of Aluminum, Alcoa Technical Paper No 19, 1987.
[54] J.Z. Mbese, P.A. Ajibade, Preparation and characterization of ZnS, CdS and HgS/Poly(methyl methacrylate) nanocomposites, Polymers (Basel) 6 (2014) 2332–2344, doi:10.3390/polym6092332.
[55] D. Han, X. Li, L. Zhang, Y. Wang, Z. Yan, S. Liu, Hierarchically ordered meso/macroporous γ-alumina for enhanced hydrodesulfurization performance, Microporous Mesoporous Mater. 158 (2012) 1–6, doi:10.1016/j.micromeso.2012.03.022.
[56] R.A. van Santen, P.W.N.M. van Leeuwen, J.A. Moulijn, B.A. Averil, Catalysis: An Integrated Approach, 1999.
[57] P. Souza Santos, H. Souza Santos, S.P. Toledo, Standard transition aluminas. Electron microscopy studies, Mater. Res. 3 (2000) 104–114, doi:10.1590/S1516-14392000000400003.
[58] R. Román, M.T. Hernández, A. Ibarra, R. Vila, J. Mollá, P. Martín, M. González, The effect of carbon additives on the dielectric behaviour of alumina ceramics, Acta Mater. 54 (2006) 2777–2782, doi:10.1016/j.actamat.2006.02.016.
[59] R. Besler, M. Rossetti Da Silva, J.J. Do Rosario, M. Dosta, S. Heinrich, R. Janssen, Sintering simulation of periodic macro porous alumina, J. Am. Ceram. Soc. 98 (2015) 3496–3502, doi:10.1111/jace.13684.
[60] F.F. Lange, Densification of powder compacts: An unfinished story, J. Eur. Ceram. Soc. 28 (2008) 1509–1516, doi:10.1016/j.jeurceramsoc.2007.12.016.
[61] J.E. Palmer, C.V. Thompson, H.I. Smith, Grain growth and grain size distributions in thin germanium films, J. Appl. Phys. 62 (1987) 2492–2497, doi:10.1063/1.339460.
[62] K. Assaker, C. Carteret, P. Durand, L. Aranda, M.J. Stébé, J.L. Blin, Hydrothermal stability of ordered surfactant-templated titania, J. Phys. Chem. C. 117 (2013) 16500–16508, doi:10.1021/jp405517w.
[63] C.F. Blanford, R.C. Schroden, M. Al-Daous, A. Stein, Tuning solvent-dependent color changes of three-dimensionally ordered macroporous (3dom) materials through compositional and geometric modifications, Adv. Mater. 13 (2001) 26–29 doi:10.1002/1521-4095(200101)13:1<26::AID−ADMA26>3.0.CO;2-S.
[64] E.S. Zouboulis, M. Grimsditch, Refractive index and elastic properties of single-crystal corundum (α-Al2O3) up to 2100 K, J. Appl. Phys. 70 (1991) 772–776, doi:10.1063/1.349633.
[65] R. Zhang, A.A. Elzatahry, S.S. Al-Deyab, D. Zhao, Mesoporous titania: from synthesis to application, Nano Today 7 (2012) 344–366, doi:10.1016/j.nantod.2012.06.012.
[66] A.S. Deshpande, D.G. Shchukin, E. Ustinovich, M. Antonietti, R.A. Caruso, Titania and mixed titania/aluminum, gallium, or indium oxide spheres: sol-gel/template synthesis and photocatalytic properties, Adv. Funct. Mater. 15 (2005) 239–245, doi:10.1002/adfm.200400220.
[67] M. Argyle, C. Bartholomew, Heterogeneous catalyst deactivation and regeneration: a review, Catalysts 5 (2015) 145–269, doi:10.3390/catal5010145.